*photonics*

MDPI

*Communication*

# Tunable Photonic Hooks Generated by a Pristine–Patchy Hybrid Microsphere Lens Group

**Hanzhou Qian [1], Jun Liu [1], Xin Liu [1], Songlin Yang [1], Caojin Yuan [2], Florence Back [3], Zengbo Wang [4], Sorin Melinte [5] and Ran Ye [1,*]**

[1] School of Computer and Electronic Information, Nanjing Normal University, Nanjing 210046, China; slyang@njnu.edu.cn (S.Y.)
[2] School of Physics and Technology, Nanjing Normal University, Nanjing 210046, China; yuancj@njnu.edu.cn
[3] Facultédes Sciences et de Médecine, University of Fribourg, CH-1700 Fribourg, Switzerland; florence.back@unifr.ch
[4] School of Computer Science and Electronic Engineering, Bangor University, Bangor LL57 1UT, UK; z.wang@bangor.ac.uk
[5] Institute of Information and Communication Technologies, Electronics and Applied Mathematics, Université Catholiquede Louvain, 1348 Louvain-la-Neuve, Belgium; sorin.melinte@uclouvain.be
* Correspondence: ran.ye@njnu.edu.cn

**Abstract**

Photonic hooks (PHs) are a specific type of curved photonic nanojet with promising applications in various fields. In this work, we propose a hybrid microsphere lens group for the effective generation and flexible tuning of PHs. The influences of the inter-sphere separation, microsphere diameter, and refractive index configuration on the focal length, peak intensity, beam waist, and bending angle of PHs were systematically investigated. The PHs obtained with the proposed method exhibit higher intensity enhancement, a narrower beam waist, and a longer propagation length than those generated by a single patchy microsphere. The results may be useful for applications including optical microscopy, optical trapping, and microfabrication.

**Keywords:** photonic hook; photonic nanojet; patchy microsphere; microsphere lens group

## 1. Introduction

The Abbe diffraction limit has long been regarded as a fundamental constraint in optical imaging, preventing conventional far-field microscopes from resolving features smaller than approximately half the illumination wavelength. Dielectric microsphere-based super-resolution imaging has attracted considerable attention as a label-free, real-time, and cost-effective nanoscopy technique. In 2009, Lee et al. first demonstrated sub-diffraction imaging using self-assembled organic molecular microlenses [1]. Subsequently, Wang et al. showed that 2–9 μm silica microspheres could resolve 50 nm features under white-light illumination, establishing microsphere nanoscopy as a promising platform for label-free super-resolution imaging [2]. Since then, significant progress has been achieved through immersion engineering [3,4], scanning imaging strategies [5,6], biologically derived microlens materials [7,8], and geometric shape engineering [9].

At the heart of microsphere-assisted imaging is the photonic nanojet, a highly localized, non-evanescent electromagnetic beam generated at the shadow-side surface of a dielectric particle under plane-wave illumination [10]. A PNJ is characterized by a sub-diffraction-limited beam waist and a propagation distance extending over several wavelengths. Although the underlying imaging mechanism is not yet fully understood [11,12], it

Check for updates

Received: 28 August 2026
Revised: 23 September 2026
Accepted: 28 September 2026
Published: 3 October 2026

**Copyright:** © 2026 by the authors. Licensee MDPI, Basel, Switzerland. This article is an open access article distributed under the terms and conditions of the Creative Commons Attribution (CC BY) license.

is widely accepted that the focal position, effective length, and full width at half maximum (FWHM) of the PNJ play critical roles in determining the resolution, imaging contrast, and working distance of microsphere-based imaging systems [13–15]. To optimize these characteristics, a variety of engineering strategies have been proposed. For example, central masking modifies the transverse wavevector distribution to generate ultra-narrow PNJs [16]; surface-patterned microspheres produce bottle beams with an extended depth of focus [17]; and antireflective bilayer coatings suppress interface reflections, thereby improving imaging quality [18].

In addition to symmetric photonic nanojets, asymmetric dielectric structures can generate curved optical beams known as photonic hooks (PHs). PHs were first predicted theoretically by Minin et al. in 2016 using trapezoidal dielectric particles [19] and were experimentally demonstrated in 2019 [20]. They originate from the combined effects of phase-velocity variations within the dielectric particle and the interference of differently refracted wavefronts. Geints et al. further revealed the crucial role of edge diffraction in PH formation [21]. In addition to their generation in air, PNJs and PHs can also be realized through plasmonic waves propagating along a metal–air interface [22,23]. Compared with PNJs, PHs offer greater flexibility in tailoring the bending angle, focal length, and beam profile [24], thereby enabling a wide range of applications, including optical manipulation, contrast-enhanced nanoscopy, etc. [25,26]. More recently, Shi et al. demonstrated that PHs generated by Janus microspheres can produce curved chirality distributions of optical vortices with tunable bending angles and chirality strengths, providing new opportunities for chiral recognition and microparticle manipulation [27]. Patchy microspheres—dielectric spheres partially coated with thin metal films—represent an effective platform for PH generation by breaking the illumination symmetry and redirecting the internal energy flow with metal films [28–30]. Patchy microspheres can be mass-fabricated using physical vapor deposition and are inherently compatible with microsphere-assisted imaging systems, making them promising candidates for practical device integration [25,29]. Nevertheless, most previous studies have focused on PH generation using a single microsphere, while PH generation and optimization based on lens groups remain largely unexplored.

In this work, we investigate the light-focusing properties of pristine–patchy microsphere lens groups using the finite-difference time-domain (FDTD) method. Two-dimensional simulation models are developed to analyze the electromagnetic field distributions, key focusing characteristics, and the underlying mechanisms responsible for PH formation in the composite lens structure. The effects of critical structural parameters, including microsphere diameter, inter-sphere separation distance, and refractive index configuration, are systematically evaluated in terms of their influence on the focal length, peak intensity, FWHM, and bending curvature of the generated PHs. The results may provide theoretical insights into the focusing behavior of composite microsphere lens groups and may be useful for developing advanced micro-optical devices for super-resolution imaging and other related photonic applications.

## 2. Simulation Methods

First, we theoretically investigated the focusing performance of a microsphere lens group. The dielectric lens group, partially coated with Ag films, was illuminated by a plane wave, and the light field on the shadow side of the lens group was simulated using the finite-difference time-domain (FDTD) method. Figure 1 shows a schematic illustration of the two-dimensional cross-sectional model used in this study. As illustrated, when a normally incident plane wave with its wavelength ranging from 400–700 nm and its $|E|^2$ normalized to unity is used as the excitation source, a highly confined light field is generated on the shadow side of the patchy microsphere. In this work, the patchy microsphere has a nominally 100 nm-thick deposited silver cap. Owing to the curved spherical surface,

the silver film adopts an elliptical-like profile: its thickness gradually decreases from 100 nm at the apex of the microsphere down to 0 nm at the cap edge, corresponding to an opening angle of 90°. This geometry is consistent with the structure reported by Zou et al. [25]. Such a configuration is favorable for practical fabrication using physical vapor deposition method and can be employed for contrast-enhanced microscopic imaging. The refractive indices of the microspheres were set to either 1.90 or 1.45, corresponding to $BaTiO_3$ (barium titanate glass, BTG) and $SiO_2$, respectively. These dielectric materials are widely used in microsphere-assisted super-resolution imaging due to their favorable optical properties [5,29]. The diameter of the pristine microsphere was fixed at 30 μm, whereas the diameter of the patchy microsphere was varied from 2 to 7 μm. The separation distance between the two microspheres was adjusted from 0 to 8 μm to investigate its effect on the characteristics of the generated photonic hook. Throughout the computational domain, a non-uniform mesh with refractive-index-dependent cell sizes was employed, with all mesh elements smaller than $\lambda/30$ to ensure numerical accuracy.

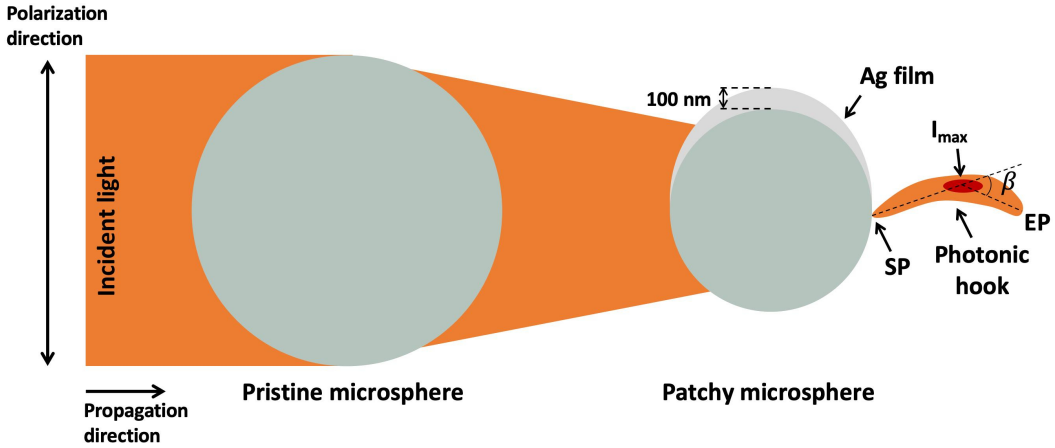



**Figure 1.** Schematic drawing of the pristine–patchy hybrid lens group and the generated photonic hook.

As shown in Figure 1, a typical PH initially has an approximately straight shape, followed by a curved intensity distribution, and finally resumes a nearly straight shape after a certain distance. The geometry of the PH can be characterized by three key points: the start point (SP), the maximum-intensity point ($I_{max}$), and the end point (EP). $I_{max}$ corresponds to the location of the maximum $|E|^2$ enhancement on the shadow side of the microsphere lens group. The EP is defined as the point along the central trajectory of the PH where the intensity decreases to $I_{max}/e$ [31,32]. To determine these characteristic points, the PH was divided into a series of slices along the propagation direction of the incident light, and the position of maximum intensity was identified in each slice. The resulting sequence of intensity maxima defines the central trajectory of the PH. The bending angle, $\beta$, is then defined as the angle between the line connecting the SP and $I_{max}$ and the line connecting $I_{max}$ and the EP.

## 3. Results and Discussion

### *3.1. Comparison of PHs Generated by Single Patchy Microspheres and Microsphere Lens Groups*

First, we compared the PHs generated by a single patchy microsphere and the proposed microsphere lens group. As shown in Figure 2a, under plane-wave illumination, a single patchy BTG microsphere generates a curved PH on its shadow side. However, the resulting PH exhibits a relatively short effective propagation length and poor spatial confinement. Its intensity decays rapidly, decreasing to $I_{max}/e$ within a very short propagation distance. Figure 2b shows the transverse $|E|^2$ intensity profile at the focal plane of the PH.

The maximum intensity reaches only 4.43, with a corresponding FWHM of approximately 656 nm.

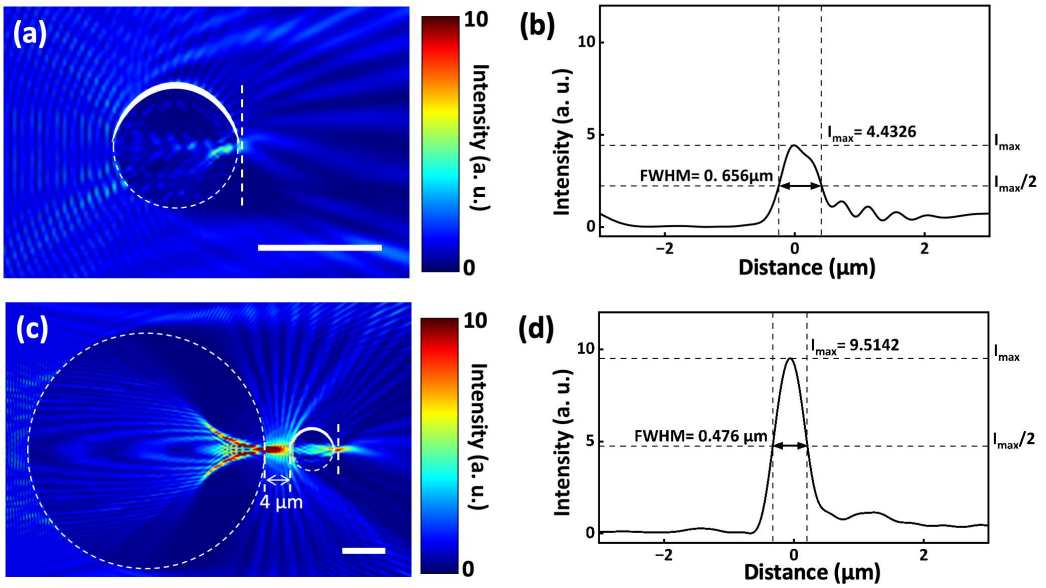



**Figure 2.** (**a**) PH formed by a single 5 μm-diameter patchy BTG microsphere with a refractive index of 1.90; (**b**) corresponding transverse intensity profile of the PH; (**c**) PH generated by a microsphere lens group consisting of a 30 μm-diameter pristine BTG microsphere and a 5 μm-diameter patchy BTG microsphere, with the separation between the two microspheres being 4 μm; (**d**) corresponding transverse intensity profile of the PH. Scale bars are 3 μm in both (**a**) and (**c**).

In contrast, as shown in Figure 2c, the proposed microsphere lens group, consisting of a pristine BTG microsphere and a patchy BTG microsphere, generates a PH with a significantly longer effective propagation length and a more well-defined curved trajectory. Owing to the prefocusing effect of the large pristine microsphere, both the propagation distance and the optical confinement of the PH are markedly enhanced compared with those of the single patchy microsphere. As quantitatively shown in Figure 2d, the peak electric-field intensity increases to 9.51, corresponding to an approximately 2.15-fold enhancement over that of the single microsphere. Meanwhile, the FWHM is reduced to approximately 476 nm, demonstrating a significant improvement in the transverse confinement of the PH.

The enhanced PH performance arises from the synergistic wavefront engineering enabled by the cascaded dual-microsphere lens architecture, which follows a similar design rationale to the microsphere lens groups previously developed for high-performance super-resolution imaging [33,34]. The underlying PH generation mechanism is also inspired by the work of Shang et al. [35], who demonstrated that PHs can be effectively generated from patchy microcylinders under point-source illumination. However, placing an independent point source within the immediate near field of a micrometer-scale particle is technically challenging and is incompatible with most conventional microscopic configurations. In the proposed hybrid lens group, the large upstream pristine microsphere serves as a lens that converts the incident plane wave into a tightly confined PNJ at its shadow-side surface. This highly localized and intense optical field effectively provides a point-source-like excitation for the downstream patchy microsphere.

Specifically, the incident plane wave is first focused by the large pristine microsphere into a tightly confined PNJ, which illuminates the downstream patchy microsphere with a diverging wavefront and substantially enhanced local intensity. Upon interacting with the patchy microsphere, part of the incident optical field is blocked by the Ag coating and reflected back into the surrounding medium. This partial reflection breaks the symmetry of

the illumination and induces an asymmetric distribution of electromagnetic energy within the microsphere. The resulting asymmetric energy flow is subsequently transformed into a curved beam upon emerging from the shadow side of the patchy microsphere, thereby generating the photonic hook [29,30].

### *3.2. Influence of the Separation Distance on the Generation and Characteristics of PHs*

Next, we investigated the influence of the inter-sphere separation distance on PH generation. As shown in Figure 3, the microsphere lens group consists of a pristine microsphere ($D = 30$ μm, $n = 1.90$) and a patchy microsphere ($D = 4$ μm, $n = 1.45$). The separation distance between the two microspheres was varied from 0 to 8 μm to evaluate its effect on the characteristics of the generated PH.

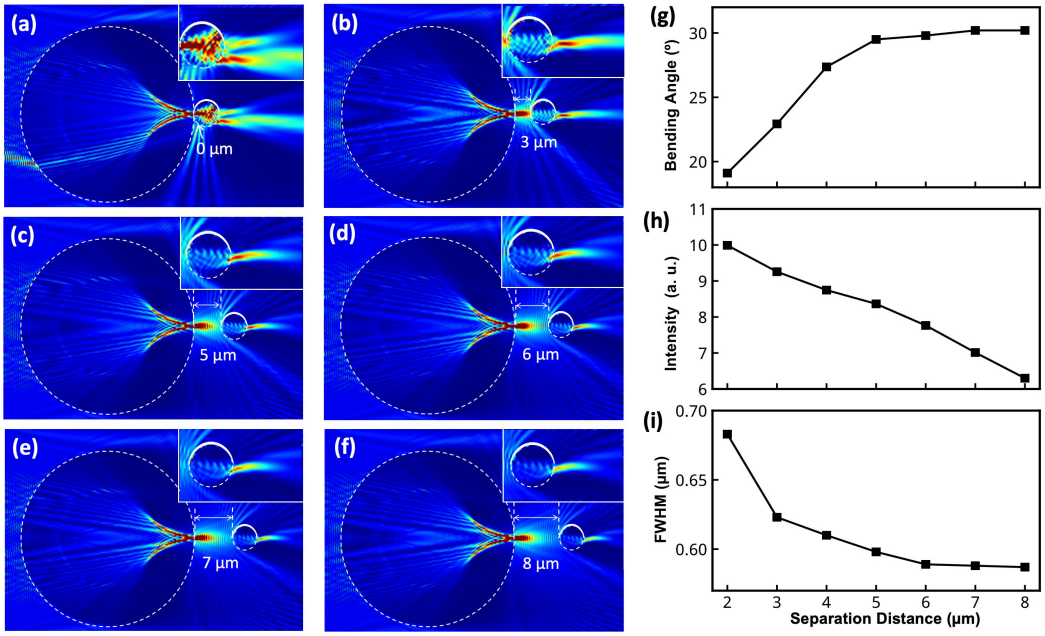



**Figure 3.** Simulated PHs generated by microsphere lens groups with different inter-sphere separation distances of (**a**) 0 μm, (**b**) 3 μm, (**c**) 5 μm, (**d**) 6 μm, (**e**) 7 μm, (**f**) 8 μm. (**g**–**i**) The corresponding evolution curves of PH characteristics as a function of inter-sphere distance: (**g**) bending angle, (**h**) $I_{max}$ and (**i**) FWHM of the PHs.

As shown in Figure 3a, when the two microspheres are in direct contact, the lens group produces a photonic nanojet accompanied by pronounced side lobes. These side lobes originate from optical interference caused by multiple reflections at the microsphere interface. When the separation distance is increased to 3 μm, the side lobes are effectively suppressed, and a well-defined PH is formed. As the separation distance increases from 3 to 5 μm, the bending angle of the PH increases rapidly. A further increase in the separation distance from 5 to 8 μm results in only minor changes to the beam profile, while the bending angle gradually stabilizes at approximately 30°, as shown in Figure 3g. This weak dependence of the PH geometry on the inter-sphere separation distance indicates that the proposed lens group is relatively tolerant to variations in the microsphere gap, thereby improving its robustness and facilitating practical implementation.

Figure 3h shows that the peak electric-field intensity ($I_{max}$) gradually decreases with increasing separation distance. As the gap widens, a smaller fraction of the optical energy emitted from the pristine microsphere is coupled into the patchy microsphere, resulting in reduced field enhancement. Quantitatively, $I_{max}$ decreases from 10.0 at a separation distance of 2 μm to 6.3 at 8 μm. Nevertheless, the reduction in peak intensity can be readily compensated by increasing the incident optical power in practical applications.

Figure 3i further shows that the FWHM decreases from 0.68 μm to 0.58 μm as the separation distance increases from 2 to 8 μm. This reduction can be attributed to the divergence of the photonic nanojet emitted by the pristine microsphere. As the photonic nanojet propagates across a larger gap, its wavefront evolves before reaching the patchy microsphere. The photonic nanojet has a better collimation after a longer propagation distance, which enables a tighter transverse field confinement by the patchy microsphere. Consequently, the generated PH exhibits a narrower beam waist and a smaller FWHM.

### *3.3. Influence of the Microsphere Diameter on the Generation and Characteristics of PHs*

Next, we investigated the influence of the patchy microsphere diameter on the characteristics of the generated PH. The refractive indices of the pristine and patchy microspheres were fixed at 1.90 and 1.45, respectively. The diameter of the pristine microsphere was maintained at 30 μm, while that of the patchy microsphere was varied from 2 to 7 μm. To ensure a consistent comparison, the inter-sphere separation distance was fixed at 4 μm throughout the simulations.

As shown in Figure 4a–f, the PH undergoes a pronounced evolution as the diameter of the patchy microsphere increases. The position of the maximum electric-field intensity ($I_{max}$), which is taken as the focal point, gradually shifts away from the shadow-side surface of the patchy microsphere, leading to an increase in the focal length, defined as the distance between $I_{max}$ and the right edge of the patchy microsphere. Figure 4g shows the dependence of the focal length on the patchy microsphere diameter. Overall, the focal length increases monotonically with increasing diameter. For a patchy microsphere diameter of 2 μm, the focal length is nearly zero, indicating that the focal point is located almost directly at the microsphere surface [Figure 4a]. As the diameter increases to 5 μm, the focal length reaches approximately 2.5 μm, and the PH exhibits its largest bending angle of approximately 30° [Figure 4d]. A further increase in the diameter to 7 μm extends the focal length to approximately 4.1 μm, accompanied by stronger localization of the optical field around the focal region.

The corresponding variations in the peak electric-field intensity ($I_{max}$) and the FWHM are presented in Figure 4h,i, respectively. In general, $I_{max}$ decreases as the patchy microsphere diameter increases, whereas the FWHM increases monotonically, indicating progressively weaker transverse confinement of the PH. For patchy microsphere diameters of 3–4 μm, the PH exhibits a distinct S-shaped trajectory. This feature results from the combined effects of surface plasmon polaritons and asymmetric energy flow [30]. A local increase in $I_{max}$ is observed when the patchy microsphere diameter reaches 6 μm. This enhancement may be attributed to stronger energy localization near the focal region as a result of the increased portion of the participated paraxial rays. However, as the microsphere diameter further increases, the light becomes less tightly confined due to more pronounced spherical aberration, causing the peak intensity to decrease while the beam width continues to increase.

### *3.4. Influence of the Microsphere Refractive Index on the Generation and Characteristics of PHs*

Furthermore, we investigated the influence of the refractive index configuration on the characteristics of the generated PH. As shown in Figure 5a, the hybrid configuration ($n_1 = 1.45$, $n_2 = 1.90$) generates a well-confined PH with a peak electric-field intensity of $I_{max} = 17.62$ and an FWHM of 0.597 μm. In contrast, when both microspheres have the same refractive index ($n_1 = n_2 = 1.45$), as shown in Figure 5b, the generated PH exhibits a slightly broader beam profile, with an FWHM of 0.604 μm and a reduced peak intensity of $I_{max} = 12.08$. The transverse $|E|^2$ intensity profiles extracted at the focal plane also quantitatively confirm these differences, as shown in Figure 5c,d.

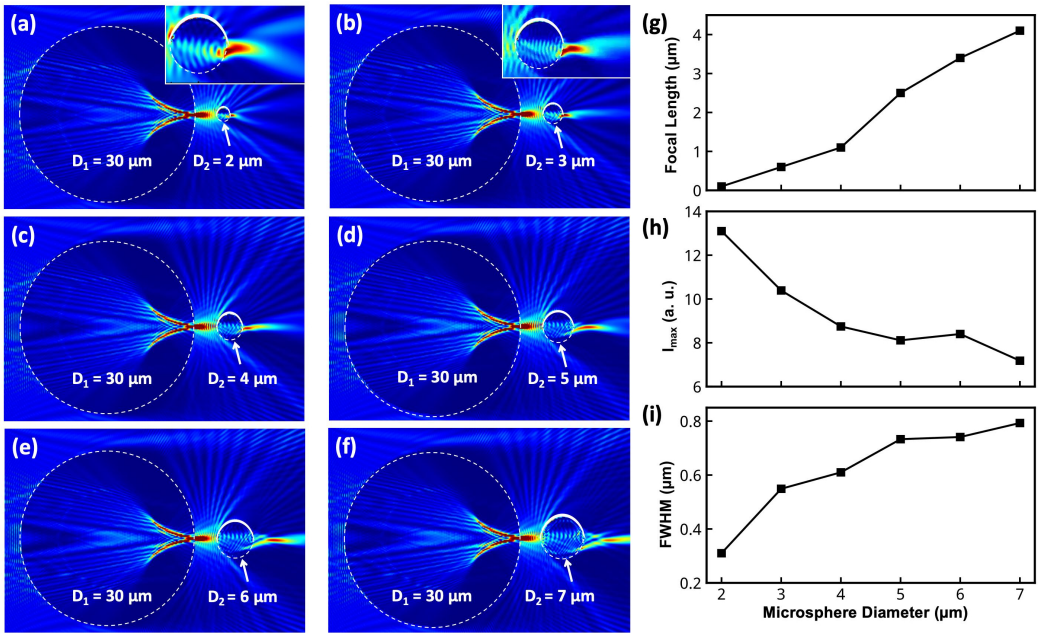



**Figure 4.** Simulated PHs generated by microsphere lens groups with patchy microsphere diameters ranging from 2 to 7 μm: (**a**–**f**) simulated $|E|^2$ field distributions; (**g**) focal length, (**h**) maximum electric-field intensity ($I_{max}$), and (**i**) FWHM of the PHs. Enlarged views of the focal region are shown as insets in panels (**a**,**b**).

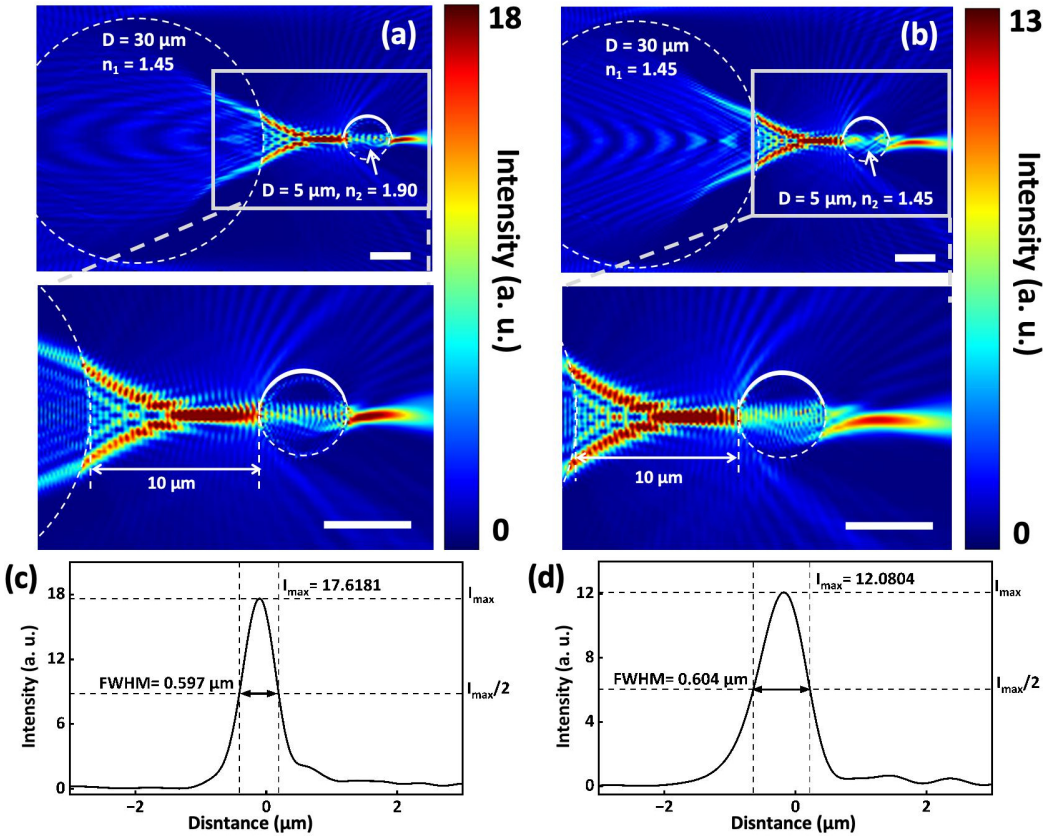



**Figure 5.** (**a**,**b**) Simulated PHs generated by microsphere lens groups with different refractive index combinations: (**a**) silica/BTG and (**b**) silica/silica; (**c**,**d**) corresponding intensity profiles extracted at the focal plane: (**c**) silica/BTG and (**d**) silica/silica. Scale bars are 5 μm.

The enhanced performance of the hybrid refractive index configuration can be attributed to the stronger focusing capability of the high-refractive-index patchy microsphere.

The larger refractive index contrast enables more efficient phase modulation and tighter transverse confinement of the optical field, resulting in a narrower PH and a higher peak intensity. In addition, the refractive index mismatch between the two microspheres modifies the optical coupling within the lens group, promoting more efficient energy localization in the hook region. By comparison, the uniform-index configuration ($n_1 = n_2 = 1.45$) provides weaker focusing and field confinement because of its lower refractive index, leading to reduced light energy localization, a lower peak intensity, and a slightly larger beam width.

### *3.5. Discussion*

One potential application of this work is super-resolution microscopy. Patchy microspheres have previously been demonstrated to enable contrast-enhanced microscopic imaging by generating oblique near-field illumination, thereby improving image contrast in microsphere-assisted nanoscopy [25,29]. Moreover, the cascaded microsphere-lens configuration employed in this study follows a similar design rationale to that of microsphere lens groups reported in previous studies, which have been experimentally demonstrated to improve imaging performance [33,34]. Beyond super-resolution imaging, the proposed system may also find applications in optical trapping and manipulation. Curved PHs can enable the non-contact manipulation of microparticles along tailored trajectories, offering potential for applications such as selective cell sorting and microfluidic particle manipulation. In particular, their curved beam trajectories can circumvent obstacles and guide target particles toward designated positions [26].

Patchy microspheres can be readily fabricated using physical vapor deposition (PVD), a standard and widely adopted technique in microfabrication. For structures with a hemispherical metallic cap, the metal film can be deposited onto individual microspheres at a glancing angle, where the oblique deposition geometry naturally produces a half-coated surface profile at the targeted region [25]. Alternatively, a smaller coated area can be achieved by exploiting the self-shadowing effect in close-packed microsphere arrays. In this approach, neighboring microspheres act as deposition masks for one another, restricting the deposition to a localized region of each particle surface and thereby producing a partial metallic coating [29].

## 4. Conclusions

In conclusion, we have proposed a strategy for generating PHs using microsphere lens groups. The characteristics of the generated PHs can be effectively tuned by controlling key parameters, including the inter-sphere separation distance, microsphere diameters, and refractive index configurations. Compared with PHs generated by a single microsphere lens, those produced by the microsphere lens group exhibit a longer effective propagation length, stronger intensity enhancement, and improved beam confinement. These results provide a simple and versatile approach for the generation and manipulation of photonic hooks, offering potential opportunities for their applications in super-resolution imaging, optical trapping, and other light–matter interaction technologies.

**Author Contributions:** Conceptualization, R.Y.; methodology, H.Q. and S.Y.; software, H.Q., J.L. and X.L.; validation, R.Y. and C.Y.; formal analysis, H.Q.; writing—original draft preparation, R.Y.; writing—review and editing, R.Y., F.B., S.M. and Z.W.; supervision, R.Y. and C.Y.; project administration, R.Y. and H.Q.; funding acquisition, R.Y., H.Q., S.M., Z.W. and C.Y. All authors have read and agreed to the published version of the manuscript.

**Funding:** This work is supported by the Postgraduate Research & Practice Innovation Program of Jiangsu Province (SJCX25_0694); the National Natural Science Foundation of China (62575141, 62505138, 62305162); Belgian Fonds de la Recherche Scientifique-FNRS (T.0126.22, U.N027.18); Royal Society APEX award (APX\R1\251114).

**Institutional Review Board Statement:** Not applicable.

**Informed Consent Statement:** Not applicable.

**Data Availability Statement:** Data underlying the results presented in this paper are not publicly available at this time but may be obtained from the authors upon reasonable request.

**Acknowledgments:** The authors thank the members of the research group for helpful discussions.

**Conflicts of Interest:** The authors declare no conflicts of interest.

## Abbreviations

The following abbreviations are used in this manuscript:

| | |
|---|---|
| PH | Photonic hook |
| PNJ | Photonic nanojet |
| FDTD | Finite-difference time-domain |
| FWHM | Full width at half maximum |
| BTG | Barium titanate glass |
| SP | Start point |
| EP | End point |

## References

1. Lee, J.Y.; Hong, B.H.; Kim, W.Y.; Min, S.K.; Kim, Y.; Jouravlev, M.V.; Bose, R.; Kim, K.S.; Hwang, I.C.; Kaufman, L.J.; et al. Near-field focusing and magnification through self-assembled nanoscale spherical lenses. *Nature* **2009**, *460*, 498–501. [CrossRef]
2. Wang, Z.; Guo, W.; Li, L.; Luk'yanchuk, B.; Khan, A.; Liu, Z.; Chen, Z.; Hong, M. Optical virtual imaging at 50 nm lateral resolution with a white-light nanoscope. *Nat. Commun.* **2011**, *2*, 218. [CrossRef] [PubMed]
3. Darafsheh, A.; Walsh, G.F.; Dal Negro, L.; Astratov, V.N. Optical super-resolution by high-index liquid-immersed microspheres. *Appl. Phys. Lett.* **2012**, *101*, 141128. [CrossRef]
4. Ye, R.; Ye, Y.H.; Ma, H.F.; Cao, L.; Ma, J.; Wyrowski, F.; Shi, R.; Zhang, J.Y. Experimental imaging properties of immersion microscale spherical lenses. *Sci. Rep.* **2014**, *4*, 3769. [CrossRef] [PubMed]
5. Wang, F.; Liu, L.; Yu, H.; Wen, Y.; Yu, P.; Liu, Z.; Wang, Y.; Li, W.J. Scanning superlens microscopy for non-invasive large field-of-view visible light nanoscale imaging. *Nat. Commun.* **2016**, *7*, 13748. [CrossRef] [PubMed]
6. Jin, G.; Bachman, H.; Naquin, T.D.; Rufo, J.; Hou, S.; Tian, Z.; Zhao, C.; Huang, T.J. Acoustofluidic scanning nanoscope with high resolution and large field of view. *ACS Nano* **2020**, *14*, 8624–8633. [CrossRef] [PubMed]
7. Monks, J.N.; Yan, B.; Hawkins, N.; Vollrath, F.; Wang, Z. Spider silk: Mother nature's bio-superlens. *Nano Lett.* **2016**, *16*, 5842–5845. [CrossRef] [PubMed]
8. Chen, X.; Wu, T.; Gong, Z.; Guo, J.; Liu, X.; Zhang, Y.; Li, Y.; Ferraro, P.; Li, B. Lipid droplets as endogenous intracellular microlenses. *Light Sci. Appl.* **2021**, *10*, 242. [CrossRef] [PubMed]
9. Wu, G.; Zhou, Y.; Hong, M. Sub-50 nm optical imaging in ambient air with 10x objective lens enabled by hyper-hemi-microsphere. *Light Sci. Appl.* **2023**, *12*, 49. [CrossRef] [PubMed]
10. Luk'yanchuk, B.S.; Paniagua-Dominguez, R.; Minin, I.; Minin, O.; Wang, Z.B. Refractive index less than two: Photonic nanojets yesterday, today and tomorrow. *Opt. Mater. Express* **2017**, *7*, 1820–1847. [CrossRef]
11. Chen, L.W.; Zhou, Y.; Li, Y.; Hong, M.H. Microsphere enhanced optical imaging and patterning: From physics to applications. *Appl. Phys. Rev.* **2019**, *6*, 021304. [CrossRef]
12. Ye, R.; Xu, C.; Tang, F.; Shang, Q.; Fan, Y.; Li, J.J.; Ye, Y.H.; Zuo, C. Simulation of the near-field focusing and the far-field imaging of microspherical lenses: A review. *Infrared Laser Eng.* **2022**, *51*, 20220086.
13. Yang, H.; Trouillon, R.; Huszka, G.; Gijs, M.A. Super-resolution imaging of a dielectric microsphere is governed by the waist of its photonic nanojet. *Nano Lett.* **2016**, *16*, 4862–4870. [CrossRef] [PubMed]
14. Yang, S.; Wang, F.; Ye, Y.H.; Xia, Y.; Deng, Y.; Wang, J.; Cao, Y. Influence of the photonic nanojet of microspheres on microsphere imaging. *Opt. Express* **2017**, *25*, 27551–27558. [CrossRef] [PubMed]

15. Darafsheh, A. Influence of the background medium on imaging performance of microsphere-assisted super-resolution microscopy. *Opt. Lett.* **2017**, *42*, 735–738. [CrossRef] [PubMed]
16. Wu, M.; Chen, R.; Soh, J.; Shen, Y.; Jiao, L.; Wu, J.; Chen, X.; Ji, R.; Hong, M. Super-focusing of center-covered engineered microsphere. *Sci. Rep.* **2016**, *6*, 31637. [CrossRef] [PubMed]
17. Zhou, Y.; Hong, M. Formation of a three-dimensional bottle beam via an engineered microsphere. *Photonics Res.* **2021**, *9*, 1598–1606. [CrossRef]
18. Wu, G.; Zhou, Y.; Hong, M. Bilayer-film-decorated microsphere with suppressed interface reflection for enhanced nano-imaging. *Opt. Express* **2022**, *30*, 28279–28289. [CrossRef] [PubMed]
19. Minin, I.; Minin, O. *Diffractive Optics and Nanophotonics: Resolution Below the Diffraction Limit*; Springer: New York, NY, USA , 2016.
20. Minin, I.V.; Minin, O.V.; Katyba, G.M.; Chernomyrdin, N.V.; Kurlov, V.N.; Zaytsev, K.I.; Yue, L.; Wang, Z.; Christodoulides, D.N. Experimental observation of a photonic hook. *Appl. Phys. Lett.* **2019**, *114*, 031105 . [CrossRef]
21. Geints, Y.E.; Minin, I.V.; Minin, O.V. Edge diffraction effect on a photonic hook generated by a dielectric microbar. *J. Opt. Soc. Am. B* **2025**, *42*, 1154–1159. [CrossRef]
22. Weisman, D.; Carmesin, C.M.; Rozenman, G.G.; Efremov, M.A.; Shemer, L.; Schleich, W.P.; Arie, A. Diffractive guidng of waves by a periodic array of slits. *Phys. Rev. Lett.* **2021**, *127*, 014303. [CrossRef] [PubMed]
23. Minin, I.V.; Minin, O.V.; Ponomarev, D.S.; Glinskiy, I.A. Photonic hook plasmons: A new curved surface wave. *Ann. Phys.* **2018**, *530*, 1800359. [CrossRef]
24. Gu, G.Q.; Zhang, P.C.; Chen, S.H.; Zhang, Y.; Yang, H. Inflection point: A perspective on photonic nanojets. *Photonics Res.* **2021**, *9*, 1157–1171. [CrossRef]
25. Zou, P.; Xu, C.; Zhi, L.; Melinte, S.; Wang, Z.; Zuo, C.; Ye, R. Photonic hook-assisted contrast-enhanced super-resolution imaging using Janus microspheres. *IEEE Photon. Technol. Lett.* **2024**, *36*, 353–356. [CrossRef]
26. Chen, W.Y.; Hung, T.Y.; Hsieh, Y.K.; Li, P.H.L.; Chen, Y.B.; Minin, O.V.; Minin, I.V.; Liu, C.Y. Numerical and experimental demonstrations of optical trapping and manipulation of a selective red blood cell using a photonic hook based on broken symmetry tapered fiber probe. *Opt. Laser Technol.* **2025**, *180*, 111520. [CrossRef]
27. Shi, Y.; Cui, Z.; Cao, X.; Minin, O.V.; Minin, I.V. Curved chirality distributions of optical vortices induced by photonic hooks. *Opt. Lett.* **2025**, *50*, 1755–1758. [CrossRef] [PubMed]
28. Tang, F.; Shang, Q.; Yang, S.; Wang, T.; Melinte, S.; Zuo, C.; Ye, R. Generation of photonic hooks from patchy microcylinders. *Photonics* **2021**, *8*, 466. [CrossRef]
29. Shang, Q.; Tang, F.; Yu, L.; Oubaha, H.; Caina, D.; Yang, S.; Melinte, S.; Zuo, C.; Wang, Z.; Ye, R. Super-resolution imaging with patchy microspheres. *Photonics* **2021**, *8*, 513. [CrossRef]
30. Xu, C.; Ye, R.; Zou, P.; Yang, T.; Melinte, S.; Wang, Z.; Zuo, C. Focusing light with a metal film coated patchy particle. *Opt. Express* **2023**, *31*, 10894–10904. [CrossRef] [PubMed]
31. Minin, I.V.; Minin, O.V.; Liu, C.Y.; Wei, H.D.; Geints, Y.E.; Karabchevsky, A. Experiments demonstration of a tunable photonic hook by a partially illuminated dielectric microcylinder. *Opt. Lett.* **2020**, *45*, 4899–4902. [CrossRef] [PubMed]
32. Liu, C.Y.; Chung, H.J.; Hsuan-Pei, E. Reflective photonic hook achieved by a dielectric-coated concave hemicylindrical mirror. *J. Opt. Soc. Am. B* **2020**, *37*, 2528–2533. [CrossRef]
33. Luo, H.; Yu, H.; Wen, Y.; Zhang, T.; Li, P.; Wang, F.; Liu, L. Enhanced high-quality super-resolution imaging in air using microsphere lens groups. *Opt. Lett.* **2020**, *45*, 2981–2984. [CrossRef] [PubMed]
34. Wu, G.; Hong, M. Optical nano-imaging via microsphere compound lenses working in non-contact mode. *Opt. Express* **2021**, *29*, 23073–23082. [CrossRef] [PubMed]
35. Shang, Q.; Xu, C.; Tang, F.; Li, J.; Fan, Y.; Yuan, C.; Wang, Z.; Zuo, C.; Ye, R. Generation of Photonic Hooks under Point-Source Illumination from Patchy Microcylinders. *Photonics* **2022**, *9*, 667. [CrossRef]


**Disclaimer/Publisher's Note:** The statements, opinions and data contained in all publications are solely those of the individual author(s) and contributor(s) and not of MDPI and/or the editor(s). MDPI and/or the editor(s) disclaim responsibility for any injury to people or property resulting from any ideas, methods, instructions or products referred to in the content.